Modeling interactions between chemistry and turbulence for simulations of partial oxidation processes

J. Caudal, Benoit Fiorina, B. Labégorre, O. Gicquel

Modeling interactions between chemistry and turbulence for simulations of partial oxidation processes

J. Caudal [a,b,c,*], B. Fiorina [a,b], B. Labégorre [c], O. Gicquel [a,b]

[a] Ecole Centrale Paris, Grande Voie des Vignes, 92290 Châtenay-Malabry, France
[b] CNRS, UPR 288, Laboratoire d'Energétique Moléculaire et Macroscopique, Combustion (EM2C), Grande Voie des Vignes, 92290 Châtenay-Malabry, France
[c] Air Liquide CRCD Paris-Saclay, 1 Chemin de la Porte des Loges, B.P. 126, 78354 Les Loges en Josas, France

Methane Autothermal Reforming (ATR) and non-catalytic partial oxidation (POX) are two industrial processes used to produce syngas, a mixture of hydrogen and carbon monoxide. In those reactors, methane is burnt with oxygen in fuel-rich conditions. Downstream of the flame, the gaseous combustion products further react with steam and remaining methane in the turbulent "post-flame" region. In order to perform Reynolds Average Navier–Stokes (RANS) simulations of the reactor, accurate modeling strategies are required to compute the average chemical source terms in this post-flame region. In the present study, a DNS numerical experiment has been performed to reproduce the properties of the flow in this part of the reactor. Results are used as a reference to a priori assess the performances of different modeling strategies derived from three turbulent combustion models. The results of this analysis show that, among the three selected models, only the two models based on tabulated chemistry description are able to properly recover the right values of the average chemical source term. The PCM-FPI approach, based on a one-point statistic description using a Beta density probability function, appears as the most accurate approach compared to the two others.

1. Introduction

A growing part of the petrochemical industry relies on the use of *syngas*, a gaseous mixture mainly composed of carbon monoxide (CO) and dihydrogen (H_2). This gas is an efficient intermediate in many processes for the production of chemicals like methanol, ammonia or dihydrogen, and is at the heart of attractive approaches for converting natural gas into liquid fuels, the so-called gas-to-liquids route.

A comprehensive survey of the major industrial processes used to obtain syngas from natural gas is proposed by Aasberg-Petersen et al. [1]. At the present time, the production of syngas from natural gas is primarily based on methane steam reforming (SMR) process. This mature technology, that produces a H_2-rich syngas, has benefited from many improvements since it was developed in the 1930s [2,3]. The endothermic global reaction for this approach is given by Eq. (1):

$$CH_4 + H_2O = CO + 3H_2 \qquad \left(\Delta H^0_{298} = -206\ \text{kJ/mol}\right). \tag{1}$$

Gasification is an alternative strategy. As explained by Higman and van der Burgt [4], it primarily refers to a partial oxidation process that is used to produce syngas from any carbonaceous fuel, which can be either solid, liquid, or gaseous. When methane is used as the feedstock, non-catalytic partial oxidation (POX) consists of burning methane with pure oxygen at elevated pressure under rich conditions, according to Eq. (2):

$$CH_4 + \frac{1}{2}O_2 = CO + 2H_2 \qquad \left(\Delta H^0_{298} = +36\ \text{kJ/mol}\right). \tag{2}$$

Autothermal reforming (ATR) is a third process which turns out to be economically particularly attractive, especially for large scale production of syngas dedicated to methanol and GTL applications [1,5,6]. This approach combines both POX and SMR processes in a single reactor, in order to use the energy released by (exothermic) partial oxidation to perform (endothermic) steam reforming. As an example, a schematic illustration of an ATR reactor is given in Fig. 1.

In processes based on partial oxidation (i.e., fuel-rich oxidation processes, like POX, ATR, and other gasification processes based on liquid or solid feedstock), reactants are usually injected separately in the reactor. Combustion takes place in a diffusion flame. Burnt gases that correspond to stoichiometric conditions (mainly CO_2 and H_2O) and remaining methane react further downstream in the so-called *Post-oxidation* zone, to produce CO and H_2. In the present paper, the results are not specific to a particular type of partial oxidation process. However, the case of ATR is of particular interest, because of the especially high water steam content in the post-oxidation region, which enhances reforming reactions. The

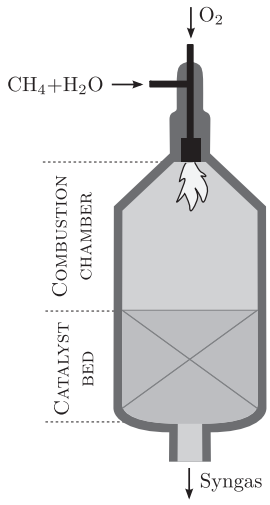

Fig. 1. Schematic illustration of an ATR reactor.

ATR process has therefore been selected to conduct the study and illustrate the reasoning.

In order to reduce the operation costs of the partial oxidation process and to increase its global efficiency, a better understanding of the flow structure and properties in the gas-phase turbulent reaction zone is required. For instance, in the ATR process, a wrong estimation of the interactions between the flame and the reactor walls could lead to a reduced lifetime of the catalyst bed and of the other equipments.

Since well-instrumented experiments are difficult to conduct on such high-pressure industrial scale reactors, numerical simulation appears as an efficient tool to address these challenges. The most accurate approach, called Direct Numerical Simulation (DNS), consists of directly solving reactive Navier–Stokes equations. However, because of the extremely high CPU cost of such simulations, DNS remains unaffordable in the case of industrial reactors. For the same reasons, Large Eddy Simulation (LES), although cheaper than DNS, is still limited to experimental studies or at best to small size pilot reactors. For large scale industrial reactors, most of the modeling works therefore rely on Reynolds Average Numerical Simulations (RANS). In this approach, the reactive flow is only described by its largest turbulent structures, and the flow balance equation is closed using numerical models.

Among these models, the turbulence/chemistry interactions (TCI) model aims at evaluating the average chemical source term. In the case of fuel-lean oxidation processes (classic combustion applications), TCI models are usually referred to as "turbulent combustion models". For partial oxidation processes, since similarities are observed with combustion processes, strategies followed up to now have been to use existing turbulent combustion models. Rehm et al. [7] modeled the interactions between chemistry and turbulence in a POX reactor using the Eddy-Dissipation Concept (EDC) developed by Magnussen [8,9]. The Eddy-Dissipation Model (EDM) [10] was also used by Amirshaghaghi et al. [11] to model chemistry evolution in the upper gaseous phase of an ATR reactor. For their part, Vegendla et al. [12] used a TCI model that relies on the use of a flamelet description, Finally, Vegendla et al. [13] and Wu et al. [14] use statistical approaches based on probability density functions (PDF) that are respectively transported [15,16] or presumed [17–19].

Among the possible modeling strategies, EDC/EDM models and presumed-PDF approaches with tabulated chemistry are low CPU time demanding. Then, these methods appear as the ablest strategies for the simulation of large-scale industrial reactors. However, Aasberg-Petersen et al. [1] pointed out that TCI models used in POX simulations often "either overestimate or underestimate the chemical reaction". This observation is also confirmed by Rehm et al. [7], who show that EDC model is extremely sensitive to its own parameters and can lead to strong errors in the evaluation of the chemical source term. Current CFD models initially developed for turbulent combustion therefore remain to be tested for POX process simulations.

The objective of the present paper is to assess, in the context of POX simulations, the performance of a selection of TCI models that were initially developed and validated for turbulent flames. Two routes for chemistry modeling are explored: detailed chemistry and tabulated chemistry. To tackle flame–turbulence interactions, detailed chemistry is coupled with the turbulent flow using EDC whereas tabulated chemistry is combined with the presumed PDF of the progress variable. The tabulated chemistry method retained here relies on the Flame Prolongation of ILDM (FPI) formalism [20]. The coupling of presumed PDF formalism (also called Presumed Conditional Moment (PCM) in the literature [19]) with FPI is noted PCM-FPI. The mathematical functions retained to presume the PDF are the Dirac and Beta functions. To summarize, three modeling combinations are tested:

- Detailed chemistry with EDC.
- PCM-FPI, with a Dirac function presumed PDF (i.e., no particular modeling of flame and turbulence interactions).
- PCM-FPI, with a Beta function presumed PDF.

Since large scale experiments on real reactors are too difficult to set up because of the severe operating conditions, the present paper proposes to evaluate the above mentioned TCI models using the results obtained in a highly resolved DNS of a 2-D representative domain.

Section 2 describes the context of RANS simulation and the strategy to compare the selected TCI models. Section 3 is dedicated to the description of the DNS simulation designed to reproduce the main properties of a POX reactor post-oxidation zone. The results obtained from this simulation are then presented in Section 4 to evaluate the ability of the selected turbulent combustion models to reproduce the expected average chemical source terms. Section 5 is dedicated to the physical analysis of the obtained results. Finally, in Section 6, a 1-D RANS simulation of the post-oxidation zone is performed to validate the results given by the a priori analysis.

2. Context and strategy of the present work

2.1. Brief overview of RANS formalism

RANS approach consists in solving averaged Navier–Stokes equations. In particular, species transport equation can be written in compressible form as following:

$$\frac{\partial \bar{\rho}\tilde{Y}_k}{\partial t} + \frac{\partial}{\partial x_j}\left(\bar{\rho}\tilde{Y}_k\tilde{u}_j\right) = -\frac{\partial}{\partial x_j}\left(\overline{\rho Y_k V_{k,j}}\right) - \frac{\partial}{\partial x_j}\left(\bar{\rho}\widetilde{u_j'' Y_k''}\right) + \bar{\dot{\omega}}_k W_k \tag{3}$$

where $\bar{A}$ and $\tilde{A}$ respectively denote Reynolds- and Favre-average of A quantity. $\bar{\rho}$ represents the average density and $\tilde{u}_j$ the jth averaged component of the velocity vector ($j = 1, \ldots, 3$). For a given species k, $\tilde{Y}_k$ refers to the averaged mass fraction, W_k to the molar mass, $\bar{\dot{\omega}}_k$ to the averaged molar chemical source term and $V_{k,j}$ to the diffusion velocity in direction j.

Several terms that appear in RANS equations are unresolved and need to be modeled. For instance, in the case of species equation (Eq. (3)), models are required to evaluate the molecular diffusion flux $\overline{\rho Y_k V_{k,j}}$, the species flux $\widetilde{u_j'' Y_k''}$ and the average chemical source term $\bar{\dot{\omega}}_k$. Many approaches have already been proposed for each of these models in the context of turbulent flames [21,22].

However, these strategies may not be valid for RANS simulations of POX processes. In particular, chemical reactions are expected to be very slow in POX post-oxidation zone, compared to oxidation reactions

in flames [12,23–25]. They should therefore interact differently with turbulence. The modeling of the mean chemical source term $\overline{\dot{\omega}}_k$ therefore appears as one of the most challenging tasks in the context of POX process simulation.

The present work aims at comparing the validity of different TCI modeling approaches initially developed for fuel-lean applications, when they are used in the post-oxidation zone of POX processes. The strategy followed to reach this objective will now be described.

2.2. Strategy adopted in the present work to compare TCI models

As stated above, experimental data that could be used to validate TCI modeling approaches are extremely difficult to obtain in a near-industrial scale facility. There is at the current time no such high-pressure plant with a sufficient set of experimental diagnostic devices. The adopted strategy is therefore to base our analyses on a highly-resolved DNS "numerical experiment".

Since DNS is very expensive in terms of CPU requirements, only a small part of the reactor chamber is simulated, which is nonetheless sufficient to reproduce a statistically pertinent flow area. The efforts are focused on a 2D-domain corresponding to the post-oxidation zone, downstream of the flame region, as illustrated in Fig. 2.

Once the DNS results are obtained, the instantaneous quantities (Y_k, T, p) are averaged and used to evaluate the TCI models as if they were obtained from a RANS solver. This strategy is referred to as a priori approach. The targeted "exact" source term, obtained by directly averaging the DNS instantaneous source term $\dot{\omega}_k$, is also evaluated and used as a reference.

A more detailed description of the DNS simulation and of how its results are used to analyze TCI models is given in Sections 3 and 4.

2.3. TCI models investigated in this study

2.3.1. PCM-FPI model

The PCM-FPI model is based on a combination of tabulated chemistry using an FPI (Flame Prolongation of ILDM) table and Presumed Conditional Moments (PCM) turbulence statistical description.

Tabulated chemistry aims at reducing the CPU cost associated with the computation of the chemical source term. The strategy consists of reducing the problem dimension by identifying a small number of degrees of freedom. A series of elementary combustion configurations is performed with a detailed kinetic scheme to construct a N_{tab}-dimensions chemical table. The chemical source term of the kth species ($k = 1, \ldots, N_s$) is then evaluated as follows:

$$\dot{\omega}_k = \dot{\omega}_k^{(\mathrm{tab})}\left(\varphi_1, \ldots, \varphi_{N_{tab}}\right) \tag{4}$$

where φ_i represents the ith coordinate ($i = 1, \ldots, N_{tab}$ with $N_{tab} \ll N_s$) of the reduced subspace on which the system evolves.

During the multidimensional simulation, one equation is solved for each φ_k variable, and the chemical source term is taken from the table when required [20,21,26–29].

In FPI methodology, the chemical trajectories are modeled by a collection of 1-D premixed flames. For adiabatic combustion, when the reactants are perfectly mixed, it has been shown that the chemical trajectories are captured by a chemical database constructed with a single premixed flamelet element. Then, thermo-chemical variables are correlated to a unique progress variable Y_c, which follows a monotonic evolution across the flame. The normalized form of the progress variable reads:

$$c = \frac{Y_c - Y_c^{\mathrm{ini}}}{Y_c^{\mathrm{end}} - Y_c^{\mathrm{ini}}} \tag{5}$$

where Y_c^{ini} and Y_c^{end} are the values of Y_c obtained at the beginning and at the end of the considered flame profile, respectively.

The FPI table used in the present work is constructed from a 1D freely propagating laminar flame simulation. The inlet boundary conditions, specified in Table 1, correspond to a mixture of methane (CH_4), oxygen (O_2) and water steam (H_2O), which is representative of the global reactant concentrations injected in ATR reactors. Fig. 3 shows the temperature and species mass fraction profiles provided by this computation and stored in the FPI table.

As explained in Section 2.2, only the post-oxidation zone of a POX process is considered. Y_c^{ini} and Y_c^{end} are therefore defined as the values of Y_c obtained at the beginning (i.e., $T = T_{\max}$) and at the end of the post-oxidation zone ($T = T_{\mathrm{equilibrium}}$), respectively. Several definitions for the progress variable are tested in Fig. 4. $Y_c = Y_{CO}$ appears adequate for the post-oxidation zone. Indeed, Fig. 4 shows that CO mass fraction evolves monotonically from the beginning ($c = 0$, $Y_{CO} = 0.20$) to the end ($c = 1$, $Y_{CO} = 0.46$) of the post-oxidation zone. The mass fraction of H_2, as well as the sum $Y_{CO} + Y_{CO_2}$, could also be a satisfactory definition for the progress variable, but CO_2 mass fraction is not adequate, since it does not evolve monotonically.

In RANS simulations, referring only to the laminar source term from FPI table is not sufficient, and turbulence effects have to be taken into account. In PCM-FPI approach, a statistical description is used by introducing a probability density function (PDF) $\widetilde{P}$:

$$\overline{\dot{\omega}}_k(\boldsymbol{x}) = \int_0^1 \dot{\omega}_k^{(\mathrm{tab})}(c^*)\,\widetilde{P}_{\boldsymbol{x}}(c^*)\,dc^*. \tag{6}$$

In the context of this paper, two types of presumed shapes for the PDF are considered:

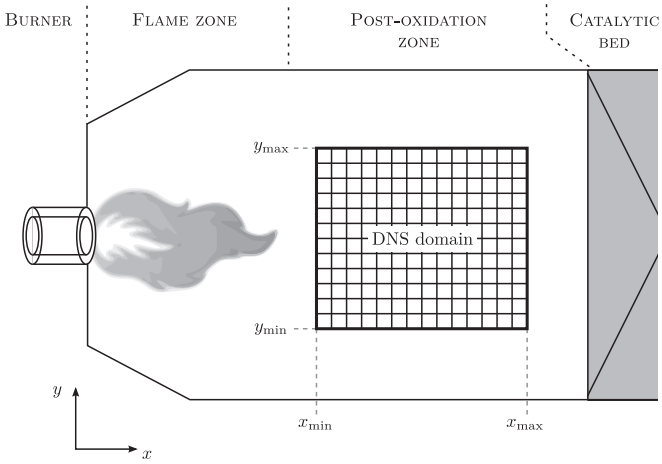

Fig. 2. Non-scaled schematic representation of the DNS domain inside an ATR reactor.

Table 1
Physical parameters describing the fresh gas properties for the reference laminar premixed flame.

Variable	Value in fresh gases
Temperature (K)	640.0
Pressure (Pa)	35.0×10^5
X_{H_2O}	0.30
X_{CH_4}	0.42
X_{O_2}	0.28
$S/C = X_{H_2O}/X_{CH_4}$	0.71
$\varphi = 2X_{CH_4}/X_{O_2}$	3.0

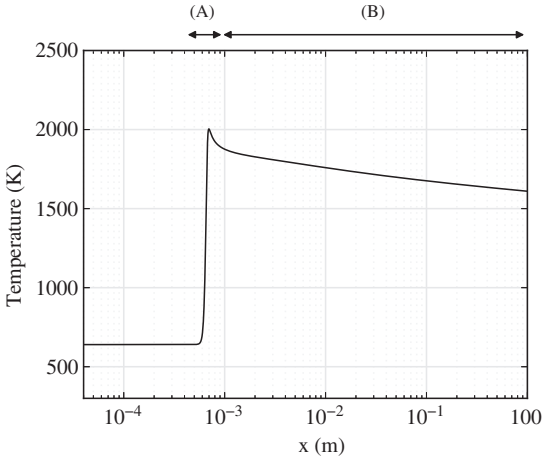

(a) Temperature

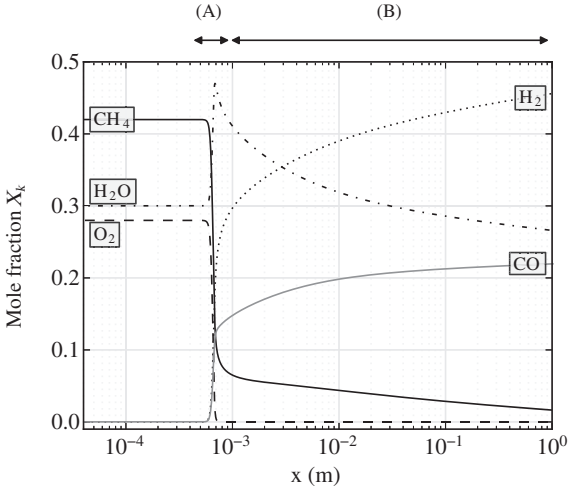

(b) Mole fractions

Fig. 3. Solutions of the 1D flamelet which constitute the FPI table. Temperature (top) and composition (bottom) are plotted in terms of the spatial coordinate x, normal to the flame front. (A) corresponds to the flame zone, (B) to the post-oxidation zone.

- A Dirac function is defined as:

$$\overline{P}_{\boldsymbol{x}}(c^*) = \delta(c^* - \widetilde{c}(x)). \tag{7}$$

This expression neglects flame/turbulence interactions and leads to the following approximation [22]: $\overline{\dot{\omega}}_k(x) = \dot{\omega}_k^{(\mathrm{tab})}(\widetilde{c}(x))$. It is a priori not appropriate for flames, but may be relevant for slow chemistry processes.

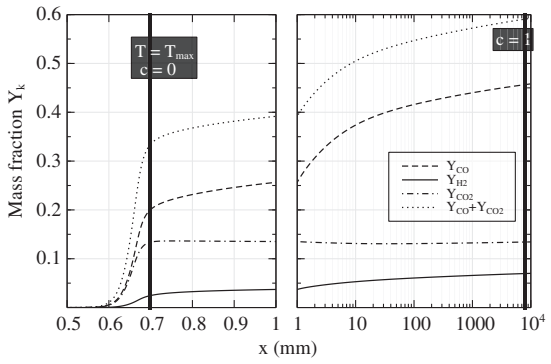

Fig. 4. Comparison of different progress variable definitions.

- A Beta function is defined as:

$$\overline{P}_{\boldsymbol{x}}(c^*) = \frac{c^{*\ \alpha_x - 1}(1-c^*)^{\beta_x - 1}}{\int_0^1 c^{\alpha_x - 1}(1-c)^{\beta_x - 1} dc.} \tag{8}$$

Parameters α_x and β_x are obtained from $\widetilde{c}(x)$ and the segregation factor $S_c(x) = (\widetilde{cc} - \widetilde{c}\widetilde{c})/(\widetilde{c}(1-\widetilde{c}))$.

2.3.2. Eddy Dissipation Concept (EDC)

The EDC formalism introduces detailed chemistry in turbulent flows. This model, which was introduced by Magnussen and Hjertager [10], has benefited from numerous improvements [8,9]. It is based on the assumption that reaction rates are controlled by turbulent mixing rates. Its principle relies on the turbulence description proposed by Tennekes [30] which divides each cell of the domain into two parts: the so-called *fine structures*, which represent a fraction γ of the fluid total mass in the cell and correspond to dissipative vortex tubes with a diameter of the order of the Kolmogorov scale, and the surrounding flow with a fraction $1 - \gamma$ of the fluid mass in the cell.

Each fine structure exchanges mass and energy with the surrounding fluid, with an exchange rate $\dot{m}$ (expressed as a fraction of the cell mass per time unit) or $\dot{m}^* = \dot{m}/\gamma$ (fraction of the fine structure exchanged per time unit). A fluid particle that enters a fine structure stays in it during a residence time defined as $\tau^* = 1/\dot{m}^*$. A part χ^* of the fine structure is also supposed to be reactive. The fine structure can thus be described as a perfectly stirred reactor (PSR) fed with particles that come from the surrounding fluid and react with time. The chemical source term of a given species k that enters this fine structure can be written in steady case:

$$\overline{\dot{\omega}}_k W_k = \overline{\rho}\dot{m}\chi^*\left(Y_k^* - Y_k^0\right) = \overline{\rho}\gamma\chi^*\left(Y_k^* - Y_k^0\right)/\tau^* \tag{9}$$

where * and ^{0} exponents respectively refer to the fine structure and the surrounding fluid quantities. In addition, the mean value of $\widetilde{Y}_k$ in the cell can be expressed as:

$$\widetilde{Y}_k = \underbrace{\chi^*\gamma Y_k^*}_{\substack{\text{Fine structures}\\ \text{Reactive part}}} + \underbrace{(1-\chi^*)\gamma Y_k^0}_{\substack{\text{Fine structures}\\ \text{Non-reactive part}}} + \underbrace{(1-\gamma)Y_k^0}_{\substack{\text{Surrounding}\\ \text{fluid}}} \tag{10}$$

$$= \chi^*\gamma Y_k^* + (1-\chi^*\gamma)Y_k^0. \tag{11}$$

By replacing in Eq. (9) the value of Y_k^0 obtained in Eq. (11), one obtains the expression of the mean source term in the EDC model:

$$\overline{\dot{\omega}}_k = \frac{\overline{\rho}\gamma\chi^*}{W_k\tau^*(1-\gamma\chi^*)}\left(Y_k^* - \widetilde{Y}_k\right). \tag{12}$$

In practice, a PSR calculation is performed in each cell using a detailed kinetics scheme, in order to obtain the steady-state value of Y_k^* in the fine structure. χ^* parameter is assumed to be 1. As proposed by [8], τ^* and γ are computed as:

$$\tau^* = C_\tau(\nu/\varepsilon)^{0.5} \quad \gamma = C_\gamma\left(\nu\varepsilon/k^2\right)^{0.5} \tag{13}$$

where ν, ε and k respectively represent the kinematic viscosity, the kinetic energy dissipation rate and the kinetic energy. Constants C_τ and C_γ are defined as

$$C_\tau = 0.41 \quad C_\gamma = 4.6 \tag{14}$$

3. Design of the DNS simulation

3.1. Description of the code

The structured solver used for this DNS simulation is based on the compressible formulation of reactive Navier–Stokes equations. A detailed kinetics scheme is used for the description of chemistry that involves 29 species and 141 reactions [31]. Molecular diffusion is computed using Hirschfelder and Curtiss approximation [32], assuming non-unity Lewis numbers. All transport properties, such as diffusion, conduction and viscosity coefficients, as well as chemical properties, are calculated with the same approach as in Chemkin library [33,34].

Time integration is performed through the splitting method proposed by Strang [35], with an explicit 4th order Runge–Kutta scheme for convection and diffusion terms and implicit 5th order Radau5 scheme [36] for chemical source terms.

The boundary conditions are implemented using NSCBC-3D formalism, a multi-component 3-D extension of the original NSCBC method proposed by Poinsot and Lele [37]. A detailed presentation is given in Coussement et al. [38].

3.2. Global overview

As explained in Section 2.2, the DNS domain corresponds to the post-oxidation zone. It begins downstream the flame zone, where there is no O_2 left. The approximate location of the DNS domain within the reactor is shown in Fig. 2.

The simulated area consists in a 2D rectangular box. A homogeneous mixture made of oxidation products exiting the flame, mixed with the remaining methane, enters the domain at $x = x_{\min}$, with a time varying turbulent velocity profile. The gases are convected through the whole domain and exit at $x = x_{\max}$. Boundary conditions located at $y = y_{\min}$ and $y = y_{\max}$ are periodic.

The size of the domain is deduced from turbulence and chemistry parameters, as explained below in Section 3.4. Because of the large integral length scale and the slow evolution of chemistry in the post-flame, it will be shown that the required domain needs to be relatively large.

As pointed out previously, chemistry in the post-oxidation zone is slower than in the flame region. As an illustration, temperature and species profiles shown in Fig. 3 are stiff in the flame region ($5 \times 10^{-4} < x < 8 \times 10^{-4}$ m) but appear much smoother in the POX zone ($x > 8 \times 10^{-4}$ m). Indeed, as detailed in Caudal et al. [24], chemical time scales can be evaluated at least 200 times larger in the post-oxidation zone (about 2×10^{-5} s) than in the flame front (below 10^{-7} s). In the work of Vegendla et al. [12], a comparable ratio between the two zones is obtained.

In the post-oxidation zone, both Kolmogorov turbulent time scale (typical value is $\tau_k \sim 10^{-3}$ s) and integral time scale ($\tau_t \sim 10^{-2}$ s) are then closer to the chemical time scales.

The global design of the DNS relies on two major hypotheses:

- Because of the high CPU cost of the simulation due to its large size and high turbulence level, a 3-D domain is not affordable. The computational domain is therefore limited to 2-D. To be representative of a realistic configuration, the turbulent scales which characterize the 2-D turbulence field used in the DNS have been chosen to be of the same order of magnitude than the ones observed in the practical industrial reactor. In this work, these scales are estimated from a 3-D RANS simulation of the whole reactor (see Section 3.4). The ratio between chemical and turbulent time scales, which governs the turbulence/chemistry interactions, is therefore preserved in this 2-D simulation. However, the shape of the turbulent structures is not preserved. The impact of this assumption should be addressed in a future work.
- In POX reactors, reactants are injected separately in the chamber. The burner and the reactor are designed in such a way that mixing time scale ($\tau_{\text{mix}} \sim 0.01$ s) is shorter than residence time ($\tau_{\text{res}} \sim 0.2$ s). Flame and mixing lengths ($l_f \sim 0.4$ m and $l_{\text{mix}} \sim 0.07$ m, respectively, evaluated from RANS simulations) are significantly shorter than the length of the reactor ($l_r \sim 1.4$ m). In this work, turbulence vs chemistry interaction is described far downstream to the flame and mixing zone. In the DNS, the inlet gases are therefore represented as a premixing of burnt gases that enter the post-oxidation zone.

The methodology retained to prescribe initial and boundary conditions for temperature, species and velocity fields is now presented.

3.3. Temperature and species fields

To build up the DNS initial condition, temperature and species mass fractions evolution in x-direction are taken from the solution of the 1-D laminar premixed flame described in Table 1 (see Fig. 3). This flame will be referred to as the "laminar reference flame". Only the post-oxidation part of the profile is used, downstream the flame front, where the concentration of O_2 is negligible and the temperature begins to decrease (see Fig. 5). This corresponds to $x = x_0 = 10^{-3}$ m in the reference flame profile. In y-direction, temperature and species fields are initialized as uniform.

At the inlet boundary condition ($x = x_{\min}$ in Fig. 2), species composition and temperature are also set uniform along the y axis. The boundary condition values are directly provided by the laminar reference flame at $x_0 = 10^{-3}$ m, as shown on Fig. 5. Fig. 5 also reveals the location of the points corresponding to $c = 0$ and $c = 1$ in FPI table.

In the present work, post-oxidation zone is assumed sufficiently far downstream of the flame so that burnt gases are well mixed. A homogeneous species composition is imposed all along the inlet. Of course, in a whole reactor simulation, a transition zone may exist between the diffusion flame and the well-mixed post-oxidation zone, where stratification may have an influence. This transition zone does not belong to the scope of this paper, and stratification effects will require further study on the subject.

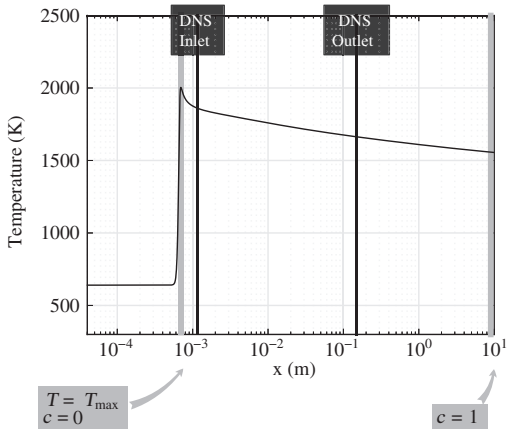

Fig. 5. 1-D temperature profile of the reference laminar premixed flame.

3.4. Turbulent velocity field

To be representative of the turbulence level that is typically found in the post-oxidation zone of a real POX reactor, the statistical properties of turbulent velocity are deduced from RANS non-reactive simulations of the whole reactor. In those simulations, the flow appears to be highly turbulent, with a turbulent Reynolds number $\mathrm{Re}_{L^i_{i,i}} = 5000$ and a turbulent intensity of 30%. The parameters resulting from these RANS computations, such as the velocity root mean square (RMS) value u' and the kinetic energy dissipation rate ε, are then used to estimate the kinetic energy spectrum that reproduces the turbulence characteristics. The shape of the spectrum is based on the work of von Karman [39] using the improvements proposed by Pao [40].

A velocity fluctuation field is then generated that verifies the properties of a homogeneous isotropic turbulence (HIT) with the identified spectrum. This HIT field is overimposed to a uniform velocity field of $3\ \mathrm{m\cdot s^{-1}}$ in the x direction. The resulting field forms the initial condition of the DNS simulation. Table 2 summarizes the main turbulence information that characterizes the flow.

A time-varying y-profile is injected in the DNS domain at $x = x_{\min}$ during the simulation, with a mean velocity of 3 m/s in the x direction. This velocity profile is extracted at any instant by linear interpolation from the HIT field used for the initial solution, and then decays throughout the DNS domain (no additional forcing is used).

3.5. Description of the mesh

In classical turbulent flame simulations, flame fronts need to be highly resolved because of the high stiffness of the chemistry. However, the computational domain considered in this study only includes the post-oxidation zone, which is characterized by large chemical length scales, as already discussed in Section 3.2. Both the time integration step and the grid size required to ensure the stability of the chemical part of the equations can therefore be chosen larger than their respective values in the flame front.

However, with an explicit integration scheme like Runge–Kutta, this would not be sufficient to ensure the stability of the computation. Thanks to the operator splitting method used in the DNS solver (see Section 3.1), the chemical part of the equations is integrated using an implicit scheme, which stabilizes the resolution. The time and grid steps are therefore not limited by chemistry but only by the resolution of turbulent convective and diffusive structures.

As recommended by Moin and Mahesh [41], the grid step is chosen of the order of magnitude of the Kolmogorov scale η_k. A structured uniform grid mesh is used in the present simulation, with $\Delta x = \Delta y = 2.4\eta_k = 2.98 \times 10^{-4}$ m.

Knowing the grid step, the lengths L_x and L_y of the domain in the x and y directions are deduced from the integral scale $L^i_{i,i}$ in order to obtain a CPU cost compatible with the available computational resources:

$$L_x = L_y = 8.0 L^i_{i,i} = 0.59\,\mathrm{m}. \tag{15}$$

The resulting number of points is $N_x = N_y = 2048$ in both directions.

The simulation was run on *Babel* IBM Blue Gene cluster at IDRIS (Institut du Développement et des Ressources en Informatique Scientifique), using 4096 cores. The total CPU cost is evaluated at 5×10^6 CPU hours.

Table 2
Physical parameters describing the properties of the homogeneous isotropic velocity field.

Parameter	Value
Parameters used for the spectrum generation	
Velocity fluctuations u' (m/s)	0.90
Dissipation rate ε ($\mathrm{m^2 s^{-3}}$)	9.66
Size of the most energetic structures l_e (m)	7.13×10^{-1}
Size of the most dissipative structures l_d (m)	4.72×10^{-4}
Other parameters describing the turbulent field	
Integral auto-correlation length scale $L^i_{i,i}$ (m)	0.075
Kolmogorov length scale l_t (m)	1.25×10^{-4}
Turbulent intensity $I = u'/\tilde{u}$	0.30
Turbulent Reynolds $\mathrm{Re}_{L^i_{i,i}}$	5000
Mean axial velocity $\tilde{u}$ (m/s)	3.00

4. Results

4.1. DNS instantaneous fields

The beginning of the steady state regime is determined by analyzing the time evolution of the length of several temperature iso-lines in the domain, as shown in Fig. 6. Fig. 6(a) shows an instantaneous view of four temperature iso-lines at $t = 0.12$ s. The evolutions of their respective lengths are presented in Fig. 6(b) as a function of time. For instance, $T = 1720$ K iso-line has a length of 0.6 m at $t = 0$, which corresponds to the size of the domain in y direction. This iso-line is then wrinkled by turbulence, and its length increases, before reaching a stable value of 1.6 m at around 0.03 s.

As an illustration, Fig. 7 shows CO mass fraction instantaneous field obtained at $t = 0.12$ s. The turbulent structures are clearly visible.

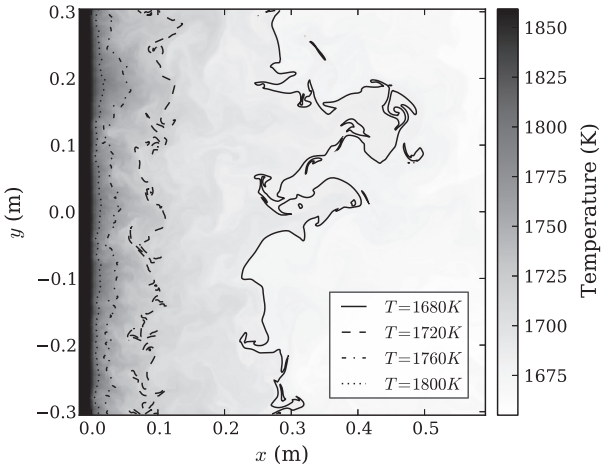

(a) Temperature field at $t = 0.12$ s

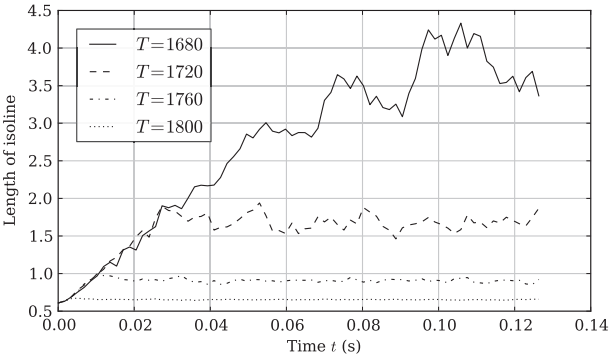

(b) Temporal evolution of the temperature iso-lines

Fig. 6. Iso-lines of temperature in the domain. Their temporal evolution is used to check whether the steady-state is reached in the domain.

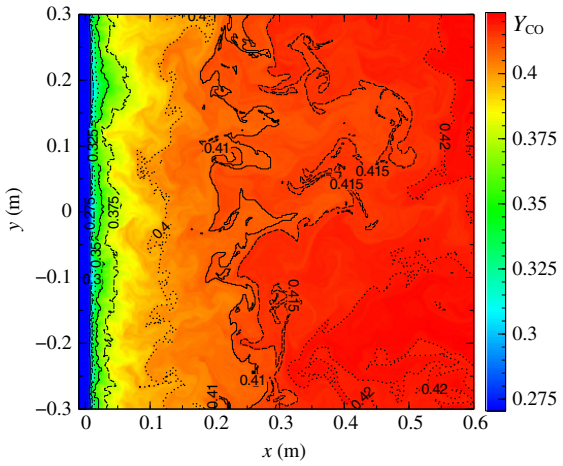

Fig. 7. 2D instantaneous view of CO mass fraction at $t = 0.12$ s.

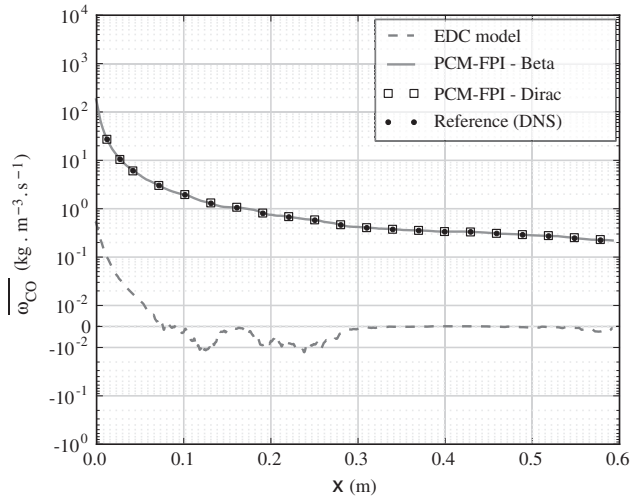

Fig. 8. Comparison of the profiles of CO mean source term obtained with various models. The black dots (●) correspond to the reference case, directly obtained from the DNS. Note that a closer comparison between Beta and Dirac approaches is shown in Fig. 14.

4.2. Definition of average from DNS results

The a priori approach used to compare RANS models using the DNS results is based on the ergodic assumption, meaning that the time statistics of the flow can be deduced from a sufficiently large instantaneous field. The time-average quantity $\bar{A}(x)$ is then evaluated as the ensemble average (denoted by the operator $\langle \cdot \rangle$) of $A(x, y)$ along y-axis for a given value of x:

$$\bar{A}(x) = \langle A(x^*, y^*) | x^* = x \rangle_{y^*} = \frac{\sum_{j=1}^{N_y} A\left(x, y_j\right)}{N_y}. \tag{16}$$

The standard deviation $\sigma_A(x)$ is also defined as:

$$\sigma_A(x) = \sqrt{\overline{A'^2}}. \tag{17}$$

The Favre-average quantities are computed as $\widetilde{A}(x) = \overline{\rho A}(x)/\overline{\rho}(x)$.

By applying these definitions to the instantaneous DNS data, 1D-profiles of mean thermochemical quantities are computed as a function of x. These average values are then used as RANS variables in order to a priori evaluate the three mean source term models presented in Section 2.3. In addition, a reference mean chemical source term $\overline{\dot{\omega}}_k(x)$ is directly obtained by averaging the DNS instantaneous values of $\dot{\omega}_k(x, y)$ using Eq. (16).

In the next section, the x-profiles of average source terms derived from the selected TCI models are compared with the reference profile $\overline{\dot{\omega}}_k(x)$.

4.3. General overview of the results

In the tabulated chemistry approach, $Y_c = Y_{CO}$ is the only transported species variable. Among chemical reaction rates, only the average source term of CO is required to perform the computation. On the contrary, models based on detailed chemistry require the correct evaluation of all species source terms.

Fig. 8 compares $\overline{\dot{\omega}}_{CO}$ predicted by the three models with the reference source term. One can observe that the models based on tabulated chemistry (PCM-FPI with Dirac and Beta functions) both recover the reference profile. On the other hand, the Eddy Dissipation Concept (EDC) underestimates the mean source term value by almost two orders of magnitude. Even the sign of the reference source term is not recovered in some areas between $x = 0.1$ and $x = 0.3$ m. Note that these conclusions are valid only for POX conditions and do not give any indication on the validity of the EDC model in other conditions (non-POX).

4.4. Further analysis of EDC model

In the EDC model, which is based on detailed chemistry, all species have to be taken into account and transported. Contrary to TCI models that rely on tabulated chemistry, all chemical source terms need therefore to be accurately evaluated. In order to assess this point, Fig. 9 shows the evolution of the positive ratio R_k defined for each species k as:

$$R_k = \left| \frac{\overline{\dot{\omega}}_k^{\,(\text{model})}}{\overline{\dot{\omega}}_k^{\,(\text{DNS})}} \right|. \tag{18}$$

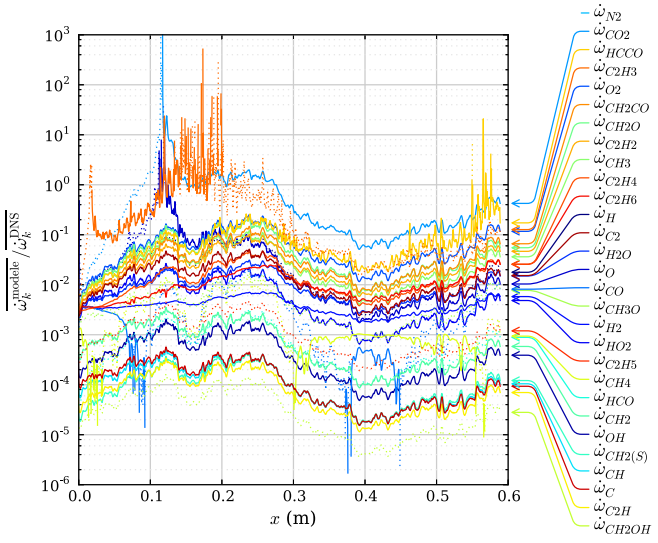

Fig. 9. Comparison of the absolute values of average source terms $\overline{\dot{\omega}}_k$ profiles for EDC model and no-model approach (with detailed chemistry). Each curve corresponds to a given species source term. Wherever the signs of both source terms are not equal, the line is drawn with dots. In the other case, the line is continuous.

For each curve, dotted parts of the line correspond to the case where $\overline{\dot{\omega}_k}^{(\text{model})}$ and $\overline{\dot{\omega}_k}^{(\text{DNS})}$ are opposite to each other, while continuous lines are used when both source terms have the same sign.

Like the CO source term, all other species source terms appear to be deeply under-evaluated by the EDC model.

5. Analysis

The results presented in Section 4 have shown that both models based on tabulated chemistry show a good agreement with the reference source term, while the EDC model is much less accurate. The present section aims at identifying the physical explanations for these results. Two main aspects have to be analyzed:

- First, the ability of the chemistry description to accurately reproduce the chemical evolution. The question is the following: "Why does FPI laminar flame tabulation work in such a turbulent case?" This point will be addressed for tabulated chemistry in Section 5.1.
- Second, the validity of the approach used to take into account the turbulence and chemistry interactions. This will be discussed in Section 5.2.

5.1. Validity of the tabulation approach

5.1.1. Identification of the reduced manifold

The DNS simulation gives access to all thermochemical states that are accessed in the computational domain at any instant t. Each of these states corresponds to a given set of instantaneous variables $(Y_1, \ldots, Y_{N_s}, T, p)$, and forms manifold dimensions at most equal to $N_s + 2$ in phase space. The tabulation approach used in the present paper assumes that only one coordinate c is necessary and sufficient to reproduce all the states reached by the system.

Fig. 10 shows a scatter plot of H_2 mass fraction obtained from the DNS field as a function of c. It reveals that all the instantaneous values of Y_{H_2} are located on a 1D trajectory in phase space, which is very close to the tabulated laminar trajectory (solid line). The same conclusion is also obtained for all other thermo-chemical quantities, which qualitatively validates the 1D evolution assumption.

To quantify the dispersion of species k mass fraction around the tabulated trajectory, the maximal relative difference $\Delta_k(x)$ between the local mass fraction $Y_k(x, y)$ and the corresponding value taken from FPI table $Y_k^{(\text{tab})}$ is evaluated along each iso-x line:

$$\Delta_k(x) = \max_y \left(\frac{Y_k(x,y) - Y_k^{(\text{tab})}(c(x,y))}{Y_k^{(\text{tab})}(c(x,y))} \right). \tag{19}$$

This quantity is less than 5% at any point in the domain and for any species k, and it stays below 1% for all major species. The present configuration is therefore characterized by a very low level of dispersion around the tabulated trajectory.

This low level of dispersion in phase space means that the physical phenomena which occur in the tabulated elementary configuration (1D laminar premixed flame in the present case) are representative of the phenomena observed in the turbulent case. For instance, this is the case in the flamelet regime, where the turbulent combustion area can be described as a set of laminar flame elements that are only wrinkled by the turbulent flow. However, in the present configuration, the flamelet regime hypothesis is not verified since the turbulent structures enter the reaction zone itself and modify the laminar structure. The low level of dispersion around the FPI trajectory can therefore only be explained by the fact that all the points evolve independently from one another because of the very low level of molecular diffusion. This point will now be discussed.

5.1.2. Evaluation of molecular diffusion

The molecular diffusion is directly linked with the gradient of species concentration, which are not necessarily the same in laminar and turbulent cases. The laminar case is useful to analyze molecular diffusion effects when no turbulence is affecting the flow. This case will be presented first. Then, the effect of turbulence on molecular diffusion will be presented.

5.1.2.1. Laminar case. In a 1-D laminar premixed flame, the steady-state species equation is composed of three terms that respectively correspond to the convective, the diffusive and the reactive parts:

$$\underbrace{\rho u \frac{\partial Y_k}{\partial x}}_{\text{Convection}} + \underbrace{\frac{\partial \rho Y_k V_k}{\partial x}}_{\text{Diffusion}} - \underbrace{\dot{\omega}_k W_k}_{\text{Reaction}} = 0 \tag{20}$$

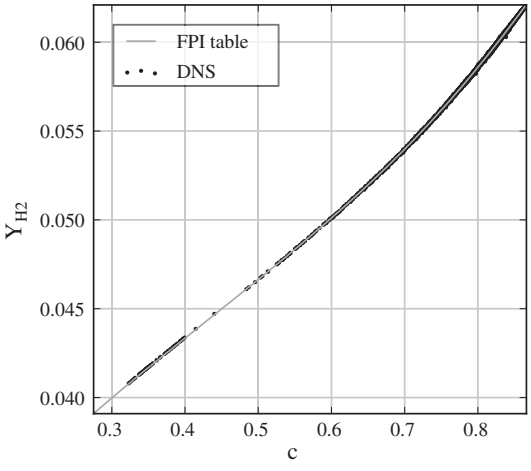

Fig. 10. Instantaneous DNS scatter plot of H_2 mass fraction as a function of c, obtained at $t = 0.12$ s. In both DNS and 1D premixed flame solvers molecular diffusion is calculated with the same non-unity Lewis number approach.

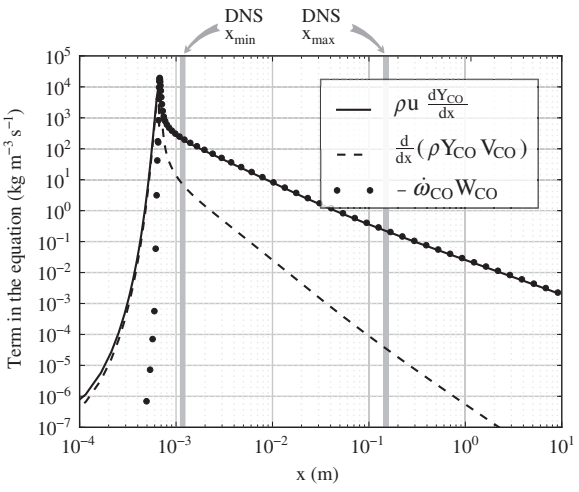

Fig. 11. Laminar profiles of the convective, diffusive and reactive terms of Eq. (20), for CO species.

where x is the direction normal to the flame front. Each of these three terms for CO equation is plotted as a function of x on Fig. 11, for the reference flame. One can notice that the diffusion terms are much lower than the two others in the post-oxidation zone. In the major part of the domain downstream of the flame ($x > 0.01$), they differ by at least two to three orders of magnitude. In the flame zone, as expected from the premixed flame theory [22,42], diffusion and chemical terms are of the same order of magnitude.

5.1.2.2. Turbulent case. The main reason why the diffusion term is very small in the laminar configuration is that the gradients of mass fractions and temperature are very small. In the turbulent case, convective transport brings fluid particles from downstream to upstream and these gradients can increase in such a way that the diffusive term may become non-negligible.

CO molecular diffusion term has therefore been evaluated on the DNS field at two different instants: $t = 0$ s, where the initial laminar profiles have not been perturbated by the turbulence yet, and $t = 0.12$ s, that correspond to an established-flow configuration. Fig. 12 shows the ratio between this diffusion term in the x direction and the CO chemical source term in the whole DNS domain.

This ratio is below 10^{-3} for $x > 0.1$ m in the laminar field ($t = 0$), but increases significantly when turbulence modifies the flow structure. Nevertheless, the diffusion term remains at least one or two orders of magnitude below the chemical source term.

As a conclusion, the very low level of diffusion in the post-oxidation zone of POX processes is responsible for an unexpected behavior of the reactive flow: each flow particle behaves in fact as if it were totally independent from its neighbors. Moreover, because of the weak influence of molecular diffusion on the chemistry, the flame archetype used for chemistry tabulation does not have a significant impact, even when the flame is turbulent. That is why the flamelet-based tabulated chemistry method gives good results in the post-oxidation zone, although the flamelet assumption regime is not satisfied. In this context, 0-D reactors would also be suitable for the chemistry tabulation.

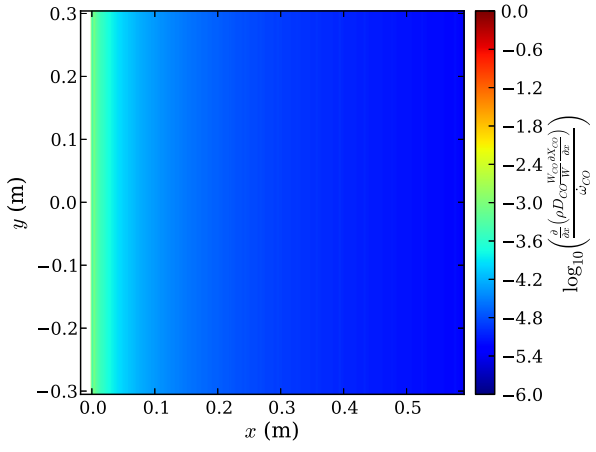

(a) $t = 0$

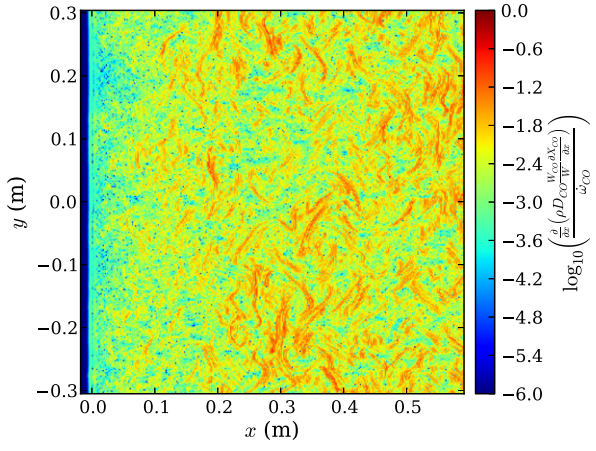

(a) $t = 0.12$ s

Fig. 12. Ratio between CO diffusion and reaction terms at two different instants.

5.2. Validity of the different strategies for describing turbulence/chemistry interactions

Tabulated chemistry has just been shown to be capable of reproducing the detailed chemical evolution in this turbulent case. The second question that now needs to be investigated is whether the different proposed strategies are able to reproduce the turbulence/chemistry interactions.

5.2.1. EDC model

As shown in Fig. 9, the Eddy-Dissipation model is not able to properly reproduce all the species source terms. This is mainly due to the use of several empirical parameters that strongly affect the value of the mean source term, as was pointed out by Rehm et al. [7].

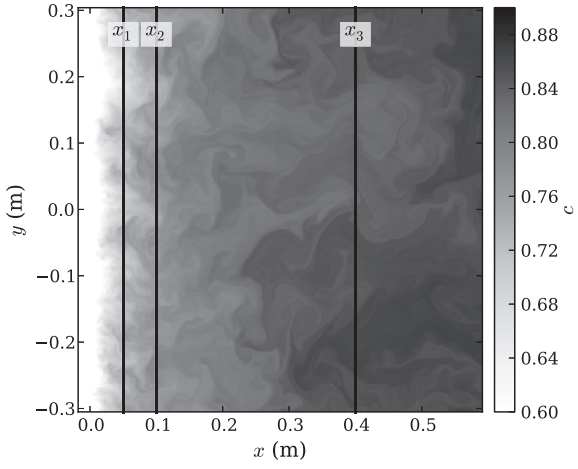

(a) c instantaneous field ($t = 0.12$ s)

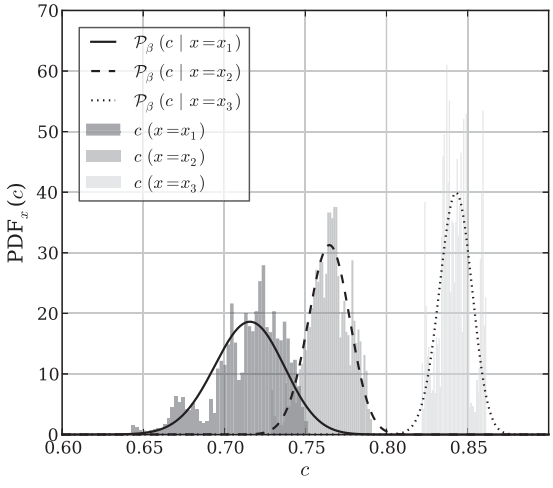

(b) β-PDF shapes and DNS statistics

Fig. 13. Comparison between the β-PDF shapes and the statistical data obtained at three locations x_1, x_2 and x_3.

The work of Rehm et al. [7] precisely aims at tuning these EDC parameters to recover the right solution in a POX simulation, but the sensitivity is so high that an optimal parameter set is difficult to obtain. Moreover, these parameters are empirical and cannot be considered universal.

5.2.2. PCM-FPI model with Beta-PDF

On the contrary, Fig. 8 shows that the Beta probability density function used in the PCM-FPI model gives very good results for estimating $\overline{\dot{\omega}_c}$. This implies that the Beta shape is a good candidate for evaluating the statistical repartition at the subgrid scale.

In order to verify this property, Fig. 13(b) shows a comparison between the β-distribution and the statistical data extracted from the DNS results at three different locations in the domain (see Fig. 13(a)). The β shapes have been evaluated with the local average ($\widetilde{c}(x)$) and fluctuation ($\widetilde{c''^2}(x)$) values of c. At the three considered locations, β-distribution appears to efficiently reproduce the statistics of the c variable, which explains why this modeling approach provides good results.

5.2.3. PCM-FPI model with Dirac-PDF

Fig. 14 shows the evolution of the error percentage $\epsilon_k^{\text{model}}$ between the modeled CO source terms and the reference one, for both tabulated approaches, the β-PDF and the δ-PDF:

$$\epsilon_k^{\text{model}} = \frac{\overline{\dot{\omega}_k^{\text{model}}} - \overline{\dot{\omega}_k^{\text{DNS}}}}{\overline{\dot{\omega}_k^{\text{DNS}}}}. \tag{21}$$

The errors obtained with these two models differ by about a factor 10, which means that the δ-PDF approach is about to provide the right order of magnitude, but is clearly less accurate than the β-PDF one.

6. RANS simulations using the identified models

The PCM-FPI approach with a β-PDF description of turbulence/chemistry interactions appears to be the most accurate for RANS simulations of the post-oxidation zone in POX reactors. All the previous results are based on a priori analyses, and it is therefore meaningful to verify this conclusion by using the identified model in a real RANS computation.

A 1D RANS computation was thus performed using a Beta-PDF based PCM-FPI model, in order to simulate the post-oxidation zone. The following equations were solved using a Newton-type solver:

$$\frac{\partial \overline{\rho}\widetilde{u}}{\partial x} = 0 \tag{22}$$

$$\overline{\rho}\frac{\partial \widetilde{Y}_c}{\partial t} + \overline{\rho}\widetilde{u}\frac{\partial \widetilde{Y}_c}{\partial x} + \frac{\partial \overline{\rho Y_c V_c}}{\partial x} + \frac{\partial \overline{\rho}\widetilde{u''Y_c''}}{\partial x} - \overline{\dot{\omega}}_{Y_c} W_c = 0. \tag{23}$$

The temperature value $\widetilde{T}$ is obtained from the FPI table.

Three terms need to be modeled in Eq. (23):

- The first one is the diffusion term $\overline{\rho Y_c V_c}$, which is determined in the following way:

$$\overline{\rho Y_c V_c} = -\overline{\rho} \overline{D} \frac{\partial \widetilde{Y}_c}{\partial x} \tag{24}$$

where $\overline{D}$ is the diffusion coefficient stored in FPI table, which was generated assuming a Lewis number Le = 1.

- The turbulent transport term $\overline{\rho}\widetilde{u''Y_c''}$ is evaluated using a gradient assumption:

$$\overline{\rho}\widetilde{u''Y_c''} = -\frac{\mu_t}{Sc_t}\frac{\partial \widetilde{Y}_c}{\partial x} \tag{25}$$

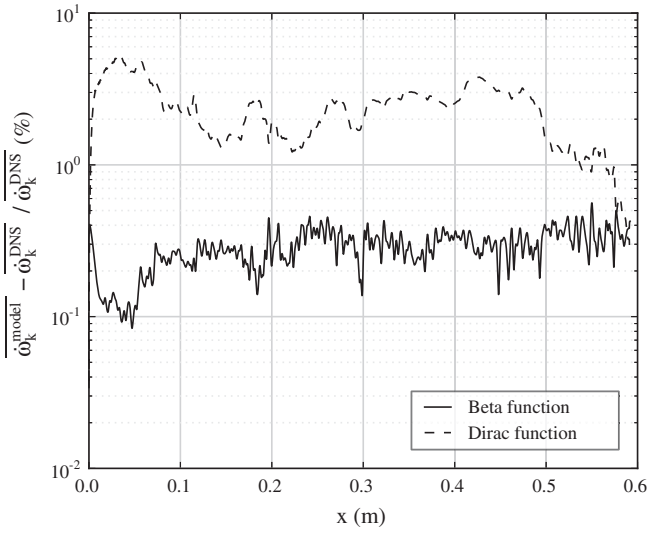

Fig. 14. Error percentage between the values of the modeled $\overline{\dot{\omega}}_{CO}$ terms and the reference values from the DNS, as defined in Eq. (21), for two different models (β-PDF and δ-PDF).

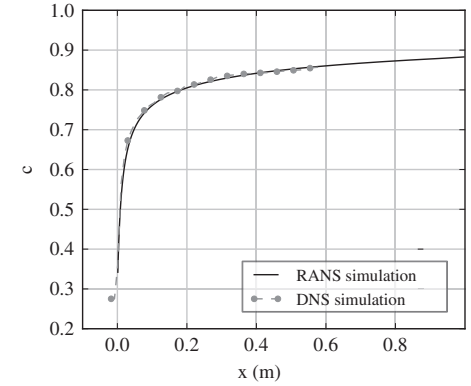

(a) Progress variable c

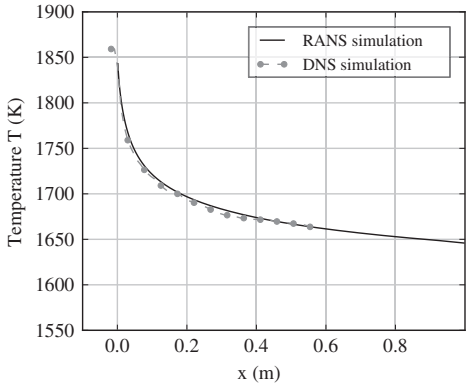

(b) Temperature

Fig. 15. Comparison between $\widetilde{c}$ and $\widetilde{T}$ profiles from 1D RANS computation and the average DNS quantities.

where the turbulent Schmidt number Sc_t is equal to 0.7 [43] and turbulent viscosity μ_t is deduced from standard $k-\varepsilon$ model:

$$\mu_t = \overline{\rho} C_\mu \frac{k^2}{\varepsilon} \quad \text{with } C_\mu = 0.09. \tag{26}$$

Kinetic energy k and its dissipation rate ε are computed using $k-\varepsilon$ theory in order to ensure the same turbulent properties as in the 2D DNS computation. For a turbulent Reynolds number $Re_t = 5000$ and a velocity fluctuation $u' = 0.9$ m/s, k and ε are given by:

$$k = u'^2 = 0.81 \quad \varepsilon = \frac{k^2}{\nu\ \mathrm{Re}_t} = 9.8\,. \tag{27}$$

- Finally, the average chemical source term $\overline{\dot{\omega}}_{Y_c} W_c$ is evaluated using a PCM-FPI approach, based on a tabulated chemistry description and a Beta probability density function. The progress variable variance is computed from the DNS and tabulated in terms of the mean progress variable. This relation is used to estimate the progress variable within the RANS computation. This methodology eliminates from the analysis the bias induced by the closure of the progress variable variance balance equation [18]. Differences between the reference DNS and the RANS are then only due to the mean chemical reaction rate modeling errors.

Average progress variable $\widetilde{c}$ and temperature $\widetilde{T}$ profiles are plotted on Fig. 15 for this RANS simulation, along with the previously presented average values from DNS computation. The length of the DNS domain is 0.58 m, while the 1D RANS simulation extends over 1 m. Both graphs show a very good agreement between RANS and DNS simulation results. This means that the conclusions drawn from the DNS a priori analysis are confirmed a posteriori by the RANS simulations.

7. Conclusion

The validity of different approaches for modeling the interaction between chemistry and turbulence in the post-oxidation zone of partial oxidation processes has been investigated.

Three models have been selected, which are based on commonly used modeling strategies for RANS simulations of industrial flames. PCM-FPI based on Beta- and Dirac-PDF both rely on a tabulated chemistry description, respectively with and without taking into account interactions with turbulence. The Eddy Dissipation Concept (EDC) model uses a turbulent mixing description of the interactions with a detailed chemical scheme.

To evaluate the ability of these three models to accurately determine the average chemical source term, a 2-D Direct Numerical Simulation (DNS) representing the turbulent flow downstream of the flame was set up. The 2-D instantaneous fields provided by the DNS were used to compute 1-D profiles of ensemble average quantities. First, this led to a set of average chemical source terms directly extracted from the DNS, which were considered the reference mean source terms. Second, the profiles of each average thermo-chemical quantity were used to compute the modeled chemical source terms for each of the three considered modeling strategies. The comparison between the reference profiles and the modeled ones allowed us to identify the most accurate approaches to model post-flame reaction rates for partial oxidation processes.

Among the three considered strategies, EDC model does not manage to properly evaluate the chemical source terms, which is mainly due to the difficulty to define a priori the right model parameters. In contrast, models based on tabulated chemistry (PCM-FPI) provide much more reliable results. Using a Dirac function as the PDF leads to a reasonable level of accuracy compared to the DNS reference, with a relative error for CO source term of a few percentage points. This relative error is further decreased by one order of magnitude with a Beta function, which therefore appears as the most promising to reproduce the interactions between chemistry and turbulence.

Finaly, a full 1D-RANS simulation was performed in order to confirm the results obtained from the a priori analysis. As expected, the PCM-FPI model was able to recover the DNS results.

Most of the RANS simulations of industrial scale reactors are obtained by using either EDC models with small kinetic schemes or tabulated chemistry. In fact, on the basis of the results that have been presented, only the models based on tabulated chemistry appear capable of correctly estimating average reaction rates in the post-oxidation zone.

However, some work still needs to be done further. First, as already mentioned above, the present work is based on the results of a 2-D simulation. In order to refine the analysis and better characterize chemistry and flow interactions, 3-D simulations should be performed. In addition, no fuel stratification has been considered in this study. Approaches based on tabulated chemistry therefore still need to demonstrate their capability to give good results when equivalence ratio heterogeneities are considered.

Acknowledgments

This work was granted access to the HPC resources of IDRIS under the allocation 2012-x2012020164 made by GENCI (Grand Equipement National de Calcul Intensif).

This work is supported by the Air Liquide chair on oxycombustion and heat transfer for energy and environment. The authors also acknowledge the support of the French Agence Nationale de la Recherche (ANR) under reference ANR-12-CHIN-0001.

References

[1] K. Aasberg-Petersen, I. Dybkjær, C.V. Ovesen, N.C. Schjødt, J. Sehested, S.G. Thomsen, Natural gas to synthesis gas — catalysts and catalytic processes, Journal of Natural Gas Science and Engineering 3 (2011) 423–459.
[2] M.A. Pena, J.P. Gomez, J.L.G. Fierro, New catalytic routes for syngas and hydrogen production, Applied Catalysis A: General 144 (1996) 7–57.
[3] K. Aasberg-Petersen, J.H. Bak Hansen, T.S. Christensen, I. Dybkjaer, P.S. Christensen, C. Stub Nielsen, S.E.L. Winter Madsen, J.R. Rostrup-Nielsen, Technologies for large-scale gas conversion, Applied Catalysis A: General 221 (2001) 379–387.
[4] C. Higman, M. van der Burgt, Gasification, 2nd ed. Gulf Professional Publishing, 2008.
[5] D.J. Wilhelm, D.R. Simbeck, A.D. Karp, R.L. Dickenson, Syngas production for gas-to-liquids applications: technologies, issues and outlook, Fuel Processing Technology 71 (2001) 139–148.
[6] I. Dybkjaer, Tubular reforming and autothermal reforming of natural gas — an overview of available processes, Fuel Processing Technology 42 (1995) 85–107.
[7] M. Rehm, P. Seifert, B. Meyer, Theoretical and numerical investigation on the EDC-model for turbulence–chemistry interaction at gasification conditions, Computers & Chemical Engineering 33 (2009) 402–407.
[8] B. Magnussen, The Eddy dissipation concept, ECCOMAS Thematic Conference on Computational Combustion, 2005.
[9] B. Magnussen, On the structure of turbulence and a generalized eddy dissipation concept for chemical reaction in turbulent flow, 19th AIAA Aerospace Science Meeting 12-15, 1981.
[10] B. Magnussen, B. Hjertager, On mathematical modeling of turbulent combustion with special emphasis on soot formation and combustion, Symposium (International) on Combustion 16 (1977) 719–729.
[11] H. Amirshaghaghi, A. Zamaniyan, H. Ebrahimi, M. Zarkesh, Numerical simulation of methane partial oxidation in the burner and combustion chamber of autothermal reformer, Applied Mathematical Modelling 34 (2010) 2312–2322.
[12] S.N.P. Vegendla, D. Messig, S. Weise, C. Hasse, Flamelet-based time-scale analysis of a high-pressure gasifier, Energy & Fuels 25 (2011) 3892–3899.
[13] S. Vegendla, G. Heynderickx, G.B. Marin, Micromixing effects on series parallel and autocatalytic reactions in a turbulent single-phase gas flow, Chemical Engineering Science 65 (2010) 4621–4629.
[14] Y. Wu, J. Zhang, P.J. Smith, H. Zhang, C. Reid, J. Lv, G. Yue, Three-dimensional simulation for an entrained flow coal slurry gasifier, Energy and Fuels 24 (2010) 1156–1163.
[15] S.B. Pope, PDF methods for turbulent reactive flows, Progress in Energy and Combustion Science 11 (1985) 119–192.
[16] D. Veynante, L. Vervisch, Turbulent combustion modeling, Progress in Energy and Combustion Science 28 (2002) 193–266.
[17] P. Libby, F. Williams, Turbulent Reacting Flows, 1994. 2–61.
[18] B. Fiorina, O. Gicquel, L. Vervisch, S. Carpentier, N. Darabiha, Premixed turbulent combustion modeling using tabulated detailed chemistry and PDF, Proceedings of the Combustion Institute 30 (2005) 867–874.

[19] L. Vervisch, R. Hauguel, P. Domingo, M. Rullaud, Three facets of turbulent combustion modelling: DNS of premixed V-flame, LES of lifted nonpremixed flame and RANS of jet-flame, Journal of Turbulence (2004) N4.
[20] O. Gicquel, N. Darabiha, D. Thévenin, Laminar premixed hydrogen/air counterflow flame simulations using flame prolongation of ILDM with differential diffusion, Proceedings of the Combustion Institute 28 (2000) 1901–1908.
[21] N. Peters, Turbulent Combustion, Cambridge University Press, 2000.
[22] T. Poinsot, D. Veynante, in: R.T. Edwards (Ed.)Theoretical and Numerical Combustion, 3rd ed., 2012.
[23] J. Caudal, Simulation numérique du reformage autothermique du méthane(Ph.D. thesis) Ecole Centrale Paris, 2013.
[24] J. Caudal, B. Fiorina, M. Massot, B. Labégorre, N. Darabiha, O. Gicquel, Characteristic chemical time scales identification in reactive flows, Proceedings of the Combustion Institute 34 (2013) 1357–1364.
[25] U. Prüfert, F. Hunger, C. Hasse, The analysis of chemical time scales in a partial oxidation flame, Combustion and Flame 161 (2) (2014) 416–426.
[26] V. Fichet, Modélisation de la combustion du gaz naturel par réseaux de réacteurs avec cinétique chimique détaillée(Ph.D. thesis) Ecole Centrale de Paris, 2008.
[27] J.V. Oijen, L. de Goey, Modelling of premixed laminar flames using flamelet-generated manifolds, Combustion Science and Technology 161 (2000) 113–137.
[28] N. Peters, Laminar diffusion flamelet models in non-premixed turbulent combustion, Progress in Energy and Combustion Science 10 (1984) 319–339.
[29] C.D. Pierce, P. Moin, Progress-variable approach for large-eddy simulation of non-premixed turbulent combustion, Journal of Fluid Mechanics 504 (2004) 73–97.
[30] H. Tennekes, Simple model for the small-scale structure of turbulence, Physics of Fluids 11 (1968) 669–671.
[31] P. Lindstedt, P. Lindstedt, Modeling of the chemical complexities of flames, Symposium (International) on Combustion 27 (1998) 269–285 (Twenty-Seventh Sysposium (International) on Combustion Volume One).
[32] J. Hirschfelder, C. Curtiss, R. Bird, Molecular Theory of Gases and Liquids, John Wiley, New York, 1954.
[33] R.J. Kee, G. Dixon-Lewis, J. Warnatz, M.E. Coltrin, J.A. Miller, Chemkin-II: a Fortran computer code package for the evaluation of gas-phase multicomponent transport properties, Technical Report, SANDIA National Laboratories, 1992.
[34] R.J. Kee, F.M. Rupley, J.A. Miller, Chemkin-II: a Fortran chemical kinetics package for the analysis of gas phase chemical kinetics, Technical Report, SANDIA National Laboratories, 1993.
[35] G. Strang, Accurate partial difference methods I: linear Cauchy problems, Archive for Rational Mechanics and Analysis 12 (1963).
[36] E. Hairer, G. Wanner, Solving ordinary differential equations, Stiff and Differential-Algebraic Problems, volume 14 of Springer series in Computational Mathematics, 2nd ed.Springer, 1996.
[37] T.J. Poinsot, S. Lele, Boundary-conditions for direct simulations of compressible viscous flows, Journal of Computational Physics 101 (1992) 104–129.
[38] A. Coussement, O. Gicquel, J. Caudal, B. Fiorina, G. Degrez, Three-dimensional boundary conditions for numerical simulations of reactive compressible flows with complex thermochemistry, Journal of Computational Physics 231 (2012) 5571–5611.
[39] T. von Karman, Progress in the statistical theory of turbulence, Proceedings of the National Academy of Sciences of the United States of America 34 (11) (1948) 530.
[40] Y.-H. Pao, Structure of turbulent velocity and scalar fields at large wavenumbers, Physics of Fluids 8 (1965) 1063–1075.
[41] P. Moin, K. Mahesh, Direct numerical simulation: a tool in turbulence research, Annual Review of Fluid Mechanics 30 (1998) 539–578.
[42] K. Kuo, Principles of Combustion, Wiley, 1986.
[43] ANSYS Fluent 12.0, User's guide, Technical Report, Ansys Inc., Lebanon, NH, USA, 2009.